Naafs, B. D. A., Monteiro, F. M., Pearson, A., Higgins, M. B., Pancost, R. D., & Ridgwell, A. (2019). Fundamentally different global marine nitrogen cycling in response to severe ocean deoxygenation. *Proceedings of the National Academy of Sciences of the United States of America*. https://doi.org/10.1073/pnas.1905553116

Fundamentally different global marine nitrogen cycling in response to severe ocean deoxygenation

B. David A. Naafs[1,*,+], Fanny M. Monteiro[2*], Ann Pearson[3], Meytal B. Higgins[4], Rich D. Pancost[1], and Andy Ridgwell[2,5]

[1]Organic Geochemistry Unit, School of Chemistry, School of Earth Sciences, the Cabot Institute for the Environment, University of Bristol, Bristol, UK

[2]School of Geographical Sciences, University of Bristol, Bristol, UK

[3]Department of Earth and Planetary Sciences, Harvard University, Cambridge, USA

[4]ExxonMobil Research & Engineering, Annandale, USA

[5]Department of Earth and Planetary Sciences, University of California-Riverside, Riverside, CA, USA

[*]These authors contributed equally

[+]Corresponding author david.naafs@bristol.ac.uk (David Naafs)

Abstract

The present-day marine nitrogen (N) cycle is strongly regulated by biology. Deficiencies in the availability of fixed and readily bioavailable nitrogen relative to phosphate (P) in the surface ocean are largely corrected by the activity of diazotrophs. This feedback system, termed the “nitrostat”, is thought to have provided close regulation of fixed N speciation and inventory relative to P since the Proterozoic. In contrast, during intervals of intense deoxygenation such as Cretaceous Ocean Anoxic Event (OAE) 2, a few regional sedimentary $\delta^{15}N$ records hint at the existence of a different mode of marine N-cycling in which ammonium plays a major role in regulating export production. However, the global-scale dynamics during this time remain unknown. Here, using an Earth System model and taking the example of OAE 2, we provide new insights into the global marine nitrogen cycle under severe ocean deoxygenation. Specifically, we find that the ocean can exhibit fundamental transitions in the species of nitrogen dominating the fixed N inventory – from nitrate (NO_3^-) to ammonium (NH_4^+) – and that as this transition occurs, the inventory can partially collapse relative to P due to progressive spatial decoupling between the loci of NH_4^+ oxidation, NO_3^- reduction, and nitrogen fixation. This finding is relatively independent of the specific state of ocean circulation and is consistent with nitrogen isotope and redox proxy data. The substantive reduction in the ocean fixed N inventory at an intermediate state of deoxygenation may represent a biogeochemical vulnerability with potential implications for past and future (warmer) oceans.

Significance statement

The ratio of the dissolved inventories of readily bio-available (fixed) nitrogen to phosphorous is regulated close to 16:1 in the modern, well-oxygenated ocean. This situation – fixed nitrogen tracking phosphorous – is generally assumed to have operated for hundreds of millions of years. Here we use computer simulations

45 combined with proxy data to instead demonstrate that the marine nitrogen cycle
46 operates very differently when dissolved oxygen concentrations in the ocean are
47 considerably lower than present. Not only is nitrate replaced by ammonium as the
48 dominant component of fixed nitrogen, but the total fixed inventory collapses relative
49 to phosphorous. This makes the strength and state of the biological pump in the
50 ocean highly susceptible to disruption, with potential past and future implications.
51 /body

Introduction

Nitrogen (N) is an essential nutrient for life, and in the modern ocean, small regional differences in the bioavailability of N induce large differences in primary productivity, ecosystem dynamics, and biogeochemical cycles (1-3). The ocean inventory of the readily bioavailable or 'fixed' forms of N, primarily nitrate (NO_3^-) and ammonium (NH_4^+), is ultimately governed by the balance between denitrification predominantly in oxygen minimum zones (OMZs) and N fixation by diazotrophs mainly in the (sub)tropical gyres (4-6). Importantly, these processes are connected on a global scale, as an increased loss of fixed N relative to phosphorus (P) favors diazotrophs that perform the energetically costly process of N fixation. As such, the marine N cycle shapes modern nutrient and ecosystem dynamics and in this system of negative feedbacks, the N:P ratio and hence fixed N inventory of the ocean are tightly regulated. Known as the "nitrostat", these feedbacks are assumed to have been relatively stable since the origin of diazotrophs in the Archaean (7) and subsequent proliferation during the (late) Proterozoic (5).

This assumption that strong negative feedbacks stabilize the oceanic N inventory, speciation, and productivity tends to frame our interpretation of future scenarios (8) and past events (9), including Oceanic Anoxic Events (OAEs). The OAEs occurred predominantly during the Mesozoic and are associated with widespread ocean deoxygenation and perturbations of major biogeochemical cycles, including the marine N cycle (10). For example, OAEs are associated with depleted bulk sediment nitrogen isotope ($\delta^{15}N_{bulk}$) values in some parts of the (proto-) Atlantic ocean (11, 12). The classical hypothesis for the operation of the marine N cycle in an extremely deoxygenated ocean – such as occurred during the OAEs – argues that primary production was dominated by diazotrophs (12, 13) to counter the high rates of N-loss in the expanded OMZs, resulting in low $\delta^{15}N_{bulk}$ values. This would be generally consistent with our understanding of a dominance of nitrostat-driven

negative feedbacks between denitrification and N fixation in the modern oceans, stabilizing the oceanic inventory of fixed N (1, 2, 4).

However, the very negative (< -2 ‰) $\delta^{15}N_{bulk}$ and even more depleted (< -4 ‰) chlorophyll-derived porphyrin N isotopes ($\delta^{15}N_{por}$) from the (equatorial) Atlantic across OAE 2 suggest a contribution, potentially major, from eukaryotic primary producers assimilating recycled ammonium (11, 14, 15). This hints at a very different operation of the marine N cycle under conditions of extreme ocean deoxygenation, in which ammonium availability may be high enough to play a major role in regulating export production, at least in the equatorial Atlantic. Similarly, very depleted $\delta^{15}N_{bulk}$ (minima ~ -3 ‰) have been found in semi-restricted shelf basins of the Tethys Ocean during the Paleocene Eocene Thermal Maximum (PETM) (16), suggesting an important role for ammonium assimilation during this transient global warming event. Together, these observations suggest that ammonium assimilation might be inherent to deoxygenation events during the Phanerozoic and may reflect the changing balance in redox speciation of the major components of dissolved inorganic nitrogen (DIN), namely: NO_3^- and NH_4^+ (together: the fixed nitrogen pool).

However, these observations highlight a major challenge: resolving the role and strength of marine N cycle feedbacks is complicated by the fact that evidence recorded in the sediments is fragmented and reflects local, not global processes (17). For OAE 2, virtually all proxy data are from the (central) Atlantic and Tethys Ocean (11). In addition, the proxy record predominantly reflects surface ocean processes, limiting our understanding of N cycle dynamics in the ocean's interior and hence the dominant reservoir of N in the intermediate and deep ocean; upwelling of this deep reservoir supports much of primary production in modern systems, and presumably in ancient ones as well. Furthermore, although models have been used to study the marine N cycle during OAE 2 (11, 15), these models have tended to either focus on a regional scale, and the area of the (proto-) Atlantic and Tethys Ocean (11), or only on the average surface vs. average deep ocean (15). Assessment of the marine N cycle

dynamics in a fully 3-dimensional and global context, as well as a more generalized understanding of how global N cycling responds to extreme ocean deoxygenation events, is still needed. To elucidate global-scale marine N cycle dynamics as the ocean is progressively deoxygenated, here we used an Earth System model of intermediate complexity ('GENIE') (18) and as a case study used Cenomanian-Turonian OAE 2 (~93 Ma), one of the most extreme ocean deoxygenation events of the last 250 Ma.

Results

In our simulations, as the oceanic P inventory increases, the associated increase in export production causes the oxygen content of the ocean to decrease, leading to expanded anoxia, here defined as < 1 nM O_2 (Fig. 1a). All simulations with more than 1 x PO_4^{3-} have enhanced export production and an expanded extent of photic zone euxinia (PZE) compared to modern, in agreement with previous box model studies (e.g., 19, 20). In the highest (4 x PO_4^{3-}) scenario, export production is more than four times higher than modern rates, and the upper depth boundaries of the OMZs impinge on the photic zone, leading to PZE in ~35% of the ocean (Fig. 1a). Within the euxinic OMZs, organic matter remineralization is predominantly mediated by sulfate reduction, contributing to 21% of total OM remineralization globally (SI Appendix, Fig. S3).

Our P inventory-induced changes in the extent of ocean oxygenation have a profound impact on the marine N cycle, and in particular, on which species of N dominates the fixed nitrogen pool: nitrate or ammonium. In our model, an increase from 0.25 to 1 x PO_4^{3-} concentration enhances primary production ~4-fold, from 2.2 to 8.6 Gt C yr^{-1}, and leads to an increase in the fixed N inventory (NO_3^- + NH_4^+) of the ocean by around 200% due to a compensating increase in N fixation (Fig. 1b-d). Notably, this is far short of the 400% increase that would have been necessary to maintain a mean N:P ocean inventory of 16:1, the reasons for which we discuss later.

The marine N cycle in the 1 x PO_4^{3-} simulation (4 x CO_2, and Cenomanian paleogeography) differs from the results for the modern (Table 1). In our Cenomanian simulations, the fixed N inventory does not reach modern values until the 4 x PO_4^{3-} simulations (Fig. 1b), highlighting the role of atmospheric CO_2 and paleogeography (affecting temperature and ocean currents, respectively) in modulating the state of marine N cycling, in addition to changes in the oceanic P inventory. In the Cenomanian simulation, higher temperatures and different ocean circulation deplete the N inventory compared to modern (Fig. 1c), implying that future warmer, deoxygenated conditions could also reduce the global ocean N inventory.

As concentrations increase towards 4 x PO_4^{3-}, the fraction of the ocean that is anoxic expands, and denitrification rates increase, resulting in up to ~15% of global organic matter being remineralized via NO_3^- respiration. The value of ~15% appears to be an inherent limit for the global contribution of denitrification to organic remineralization (SI Appendix, Fig. S3). This, in turn, places a limit on the loss of fixed N and ultimately leads to a maximum contribution of N fixation to export production of ~55-60% for an ocean with widespread anoxia but operating under an oxygen-rich atmosphere (Fig. 1d). This limit is due to geographic restriction of denitrification, which mainly occurs at the edge of the OMZs, where oxygen is low enough for denitrification, yet nitrification rates remain high enough to produce nitrate. As oxygen content in the ocean decreases, higher rates of denitrification, combined with lower nitrification rates, result in a sharp decline in nitrate concentration, reducing the eventual contribution of upwelled nitrate to export production (Fig. 1b-d).

Because nitrification of NH_4^+ requires oxygen, NH_4^+ accumulates in the ocean, mostly in the OMZs. In the 4 x PO_4^{3-} ocean, average NH_4^+ concentrations reach up to two orders of magnitude higher than in the modern ocean (Fig. 1b), reaching values similar to those observed in the modern OMZ of the Black Sea (21). In such an “ammonium ocean”, NH_4^+ assimilation does not dominate the source of

163 nutrient nitrogen for export production globally, constituting at most 22% of total
164 export production (Fig. 1d). This is because most of the upwelled NH_4^+ is nitrified in
165 oxygenated layers underlying the photic zone. However, where local NH_4^+
166 assimilation occurs, it can contribute > 30% of export production, for example in the
167 tropical proto-Atlantic. The relative contribution of N fixation and NH_4^+ assimilation to
168 export production is thus controlled by the spatial structure of the OMZ relative to the
169 base of the photic zone, which in turn is controlled by ocean circulation (i.e.,
170 upwelling regions). When the OMZ impinges the photic zone, NH_4^+ becomes
171 available for direct assimilation by phytoplankton. When the OMZ is spatially
172 separated from the photic zone, nitrification (and subsequent denitrification) reduce
173 the availability of NH_4^+ to the photic zone.
174 However, our results collectively demonstrate that the system does not
175 monotonically transition from a “nitrate” to an “ammonium” ocean as oxygen
176 progressively declines. Under intermediate conditions in the transition (in our
177 Cenomanian simulations: 2 x PO_4^{3-}), a unique state of N cycling occurs in which the
178 ocean is not yet anoxic enough to develop extensive OMZs rich in ammonium.
179 Relatively high rates of nitrification restrict the accumulation of NH_4^+, yet at the same
180 time, high rates of denitrification keep the ocean nitrate inventory low (Fig. 1d). As a
181 result, the ocean becomes extremely depleted in all forms of fixed N (Fig. 1c).
182
183 **Discussion**
184 Contrary to earlier studies (22, 23), our results show how the deep ocean can
185 become highly depleted in fixed N (Fig. 2b) relative to P, leading to a biogeochemical
186 state that contrasts markedly to the modern oxic ocean. As P concentrations
187 increase and anoxia expands, the ocean transitions from a feedback-balanced
188 system where the nitrate inventory tracks phosphate (24), to a state in which the
189 deep ocean becomes highly depleted in fixed N relative to P (Fig. 1c). And rather
190 than a NO_3^--replete deep ocean (Fig. 3a), the dominant form of nitrogen becomes

191 NH_4^+, which is furthermore localized to expanded OMZs and does not "fill" all of the
192 deep ocean (Table 1 and Fig. 3b-c). This transformation occurs in the model despite
193 high rates of N fixation at the surface by diazotrophs and concomitantly high export
194 production fluxes of particulate organic nitrogen into the ocean interior – both factors
195 that should favor a large deep ocean fixed N inventory of NH_4^+ released from organic
196 matter remineralization.

197 But did an ocean state such as this really develop in the past? Proxy data for
198 bottom water anoxia and photic zone euxinia during OAE 2 best match the 2 x PO_4^{3-}
199 simulation (25). Although there are a number of uncertainties and caveats associated
200 with both the model simulations and proxy data, the 2 x PO_4^{3-} scenario also is the
201 same scenario that yields a marine N cycle simulation with minimum total fixed N
202 inventory (Fig. 1c). In this simulation, 11% of the total volume of the ocean and 17%
203 of the sea floor is anoxic (defined here as < 1 nM O_2) (Fig. 1a and Table 1),
204 consistent with uranium isotope data that indicate that 8-15% of the sea floor became
205 anoxic during OAE 2 (26). We argue that the existence of an elevated oceanic P
206 inventory compared to the modern is consistent with calcium isotope measurements.
207 The calcium isotope data indicate an increased weathering flux during OAEs (27)
208 and as total calcium and P concentrations can be correlated in modern rivers (28),
209 presumably reflect an increased rate of PO_4^{3-} supply to the ocean. Together with the
210 likelihood that P was more strongly regenerated from the ocean floor under anoxic
211 conditions (29), an increased PO_4^{3-} state is a reasonable outcome, and the relatively
212 conservative 2 x PO_4^{3-} amplification (rather than 3 x or 4 x PO_4^{3-}) is the scenario that
213 leads to the greatest reduction in fixed N inventory.

214 In the 2 x PO_4^{3-} simulations, N fixation is the most intense in equatorial
215 upwelling regions and in the Pacific sector of the Southern Ocean, where deep and
216 denitrified waters with low N:P ratios reach the photic zone (Fig. 2). Globally, NH_4^+-
217 assimilation is significant but is not the dominant source of nutrient nitrogen for
218 marine production, contributing ~10% of total export production (Table 1). Regionally,

however, NH_4^+-assimilation is important in the most intensely anoxic and/or upwelling regions, such as the euxinic equatorial Atlantic (Fig. 2).

Available nitrogen stable isotope data for OAE 2 allow for comparison with our model simulations, although published data to date are restricted to the (proto)-Atlantic and Tethys Ocean. Records from the equatorial Atlantic (Demerara Rise sites and Site 367) show extremely depleted $\delta^{15}N_{bulk}$ values during OAE 2, with minima of < -3‰ and average values around -2‰ (13-15). These depleted $\delta^{15}N$ values are interpreted to reflect a region dominated by N fixation and/or NH_4^+ assimilation, although it is difficult to disentangle the individual importance of these two processes (15). Our model simulations are in concordance, with a relatively large contribution of N fixation and especially NH_4^+ assimilation (> 30 %), to export production in this region (Fig. 2a). By contrast, the continental margins of Europe and North America are characterized by enriched ($\delta^{15}N_{bulk}$ values around 1‰), even during the peak of OAE 2 (11). This is also consistent with our simulations, which indicate a low contribution of N fixation and NH_4^+ assimilation to export production on those particular margins, with productivity instead dominated by NO_3^-. Sites in the subtropical Atlantic (Sites 386, 1276, and 641) (11) are characterized by negative $\delta^{15}N_{bulk}$ values (average values around -1‰), although less negative then those recorded in the equatorial Atlantic (averages around -2‰). Our simulations are largely consistent with these intermediate $\delta^{15}N_{bulk}$ values, as the surface ocean at Sites 368 and 641 is characterized by a high contribution of N fixation to export production (> 50 %), but no major influence of ammonium assimilation. Site 1276 is an exception to the general agreement between our model simulations and published interpretations of $\delta^{15}N_{bulk}$ proxy data. In our simulations, this location is not characterized by high contributions of N fixation and/or NH_4^+ assimilation that would lead to depleted $\delta^{15}N_{bulk}$, yet the available $\delta^{15}N_{bulk}$ values are negative. This could be because the resolution of cGENIE is insufficient to reconstruct small-scale features in ocean circulation or biology that drive the $\delta^{15}N_{bulk}$ values at Site 1276 negative. But

overall our simulations compare well with the proxy record from the Atlantic and Tethys Ocean as well as regional box modelling studies (11, 14, 15, 30), providing additional confidence.

Both the proxy record and previous box modelling studies are limited to the Atlantic and Tethys Ocean. Our global ocean simulations suggest that NH_4^+-assimilation may have fueled export production in parts of the eastern equatorial Pacific, and that N fixation was important across the equatorial Pacific and Indian Ocean and in the high-latitude southern Pacific Ocean, regions characterized by stronger exchanges between the deep and the surface ocean. However, formal assessment of these model predictions will have to await new data from these basins, and higher resolution ocean biogeochemical modelling.

If the marine N cycle of OAE 2 can maintain a fundamentally different structure from the modern version, one might expect comparably different N cycle states to occur at other times in Earth history. For example, late Devonian black shales (31) as well as Paleocene Eocene Thermal Maximum (PETM) black shales (16) are characterized by depleted $\delta^{15}N_{bulk}$ values similar to those reported for OAE 2. The climate state and paleogeography, which determine the specific sensitivity of the marine N cycle to changes in oxygenation state, were different during those events compared to OAE 2. However, the same mechanisms and feedback processes identified for the OAE 2 scenario presumably would operate. If the anoxia was intense enough, these events also may have promoted a depletion in bio-available N; and incorporation of ammonium may have been important in euxinic (semi)-restricted basins (e.g., the Northeast Tethys during the PETM).

Changing the global N inventories and spatial patterns of N cycling also has far-reaching implications for marine ecology and attendant proxies, and other biogeochemical cycles. For example, the habitat for ammonia-oxidizers (e.g., Thaumarchaeota) may have been very different in a reorganized, low-oxygen N cycle. These organisms may have moved to shallower depths if they were able to

resist photoinhibition and other associated oxidative pressures. This shift in habitat may then influence TEX_{86}-based temperature estimates in anoxic basins, as existing calibrations are based on modern systems in which the organisms primarily reside below the base of the photic zone. Marine N_2O production likely would also have increased during anoxic events due to elevated rates of both denitrification and nitrification, and a potential shift between denitrification and anammox (32), which characterize some of the main pathways of N_2O production in the ocean (33). If the N_2O cycle shifted closer to surface waters, thereby increasing gas evasion rates, N_2O could have provided a powerful positive feedback mechanism to sustain the OAE. N_2O is a potent greenhouse gas, 1000 times more effective than CO_2, and its release could partially offset the negative feedback on warming of the expansion in organic carbon burial. The interplay of such processes could account for the rather complex temperature changes observed across OAE 2 (34). Besides the biogeochemical implications, these changes in the marine N cycle likely also impacted marine trophic structures and food webs and could be an important mechanism for how deoxygenation events such as the OAEs drive biological turnover

The scenarios modeled here may also have important implications for future climate change. Over the past 50 years the oxygen content of the ocean has declined (35) and is expected to accelerate with future ocean warming (36). Some regions of the ocean are already close to transitioning to full anoxia (<10 nM O_2) (37). Our results illuminate the sensitivity of the marine N cycle to changes in ocean oxygen content, implying that the future ocean may be more vulnerable to N loss than previously recognized, which will have far-reaching consequences for other biogeochemical processes and marine ecosystems.

Conclusions

Our understanding of the response of the marine N cycle to changes in ocean oxygenation largely comes from past perturbation events such as the Ocean Anoxic

Events of the Mesozoic, with relatively sparse proxy records and regional models informing most of our understanding to date. Here, we applied an Earth system model with 3D global ocean (GENIE), upgraded with a more complete set of N cycle processes, to provide specific insights into the global marine N-cycle associated with OAE 2 as well as to provide generalized understanding of how the marine N cycle responds under progressively extreme deoxygenation. We find that as phosphate concentrations increase and anoxia expands, the ocean transitions from an oxic state with high concentrations of nitrate to an anoxic/reducing state in which the deep ocean becomes highly depleted in fixed N relative to P, with N predominantly in the form of ammonium and mostly geographically restricted to expanded OMZs. These results point to potential breakdown in the feedbacks that were thought to keep global N marine inventories in balance, i.e., the “nitrostat”.

Materials and Methods

All simulations were run using the GENIE model. As employed here, GENIE includes representations of the marine cycles of phosphorus, nitrogen, oxygen, and sulfur. To extend the applicability of GENIE to a poorly oxygenated ocean, we further developed the N cycle to include second-order substrate limitation of nitrification rates by both ammonium and oxygen rather than just ammonium (see SI Appendix).

Data availability

The code for the version of the GENIE model used in this paper (technically: cGENIE) can be found here: https://svn.ggy.bris.ac.uk/subversion/genie/tags/cgenie-NaafsMonteiro.PNAS.2019 (svn revision 10275) and includes all configuration and boundary condition files (check genie-userconfigs/MS/PNAS2019.NaafsMonteiro for the specific userconfig files). The code on the SVN repository can be accessed with the username: *genie-user* and password: *g3n1e-user*. Documentation on running the cGENIE model can be found in the genie-docs directory of the code installation.

Acknowledgments

We thank S. Greene for providing the paleolocations of the sites used in this study. B.D.A.N. is funded through a Royal Society Tata University Research Fellowship. F.M.M. is supported by a NERC research fellowship (NE/J019062/1) and a NERC standard grant (NE/N011112/1). A.P. acknowledges support from the Gordon and Betty Moore Foundation, the NASA Astrobiology Institute, and a Benjamin Meaker Visiting Professorship, University of Bristol. R.D.P. acknowledges the Royal Society Wolfson Research Merit Award. This material is based on work supported by the National Science Foundation under Grant Number 1736771 (to A.R.). A.R. also acknowledges funding from the European Research Council as part of the "PALEOGENiE" project (ERC-2013-CoG-617313).

References

1. Voss M, *et al.* (2013) The marine nitrogen cycle: recent discoveries, uncertainties and the potential relevance of climate change. *Phil. Trans. R. Soc. B* 368(20130121).
2. Moore CM, *et al.* (2013) Processes and patterns of oceanic nutrient limitation. *Nature Geosci.* 6(9):701-710.
3. Falkowski PG, Barber RT, & Smetacek V (1998) Biogeochemical Controls and Feedbacks on Ocean Primary Production. *Science* 281(5374):200.
4. Redfield AC (1958) The biological control of chemical factors in the environment. *Am. Sci.* 46(3):230A-221.
5. Tyrrell T (1999) The relative influences of nitrogen and phosphorus on oceanic primary production. *Nature* 400(6744):525-531.
6. Deutsch C, Sarmiento JL, Sigman DM, Gruber N, & Dunne JP (2007) Spatial coupling of nitrogen inputs and losses in the ocean. *Nature* 445(7124):163-167.
7. Stüeken EE, Buick R, Guy BM, & Koehler MC (2015) Isotopic evidence for biological nitrogen fixation by molybdenum-nitrogenase from 3.2 Gyr. *Nature* 520:666.
8. Gruber N & Galloway JN (2008) An Earth-system perspective of the global nitrogen cycle.451:293.
9. Boyle RA, *et al.* (2013) Nitrogen cycle feedbacks as a control on euxinia in the mid-Proterozoic ocean. *Nat. Commun.* 4:1533.
10. Jenkyns HC (2010) Geochemistry of oceanic anoxic events. *Geochem. Geophy. Geosy.* 11(3):Q03004.
11. Ruvalcaba Baroni I, van Helmond NAGM, Tsandev I, Middelburg JJ, & Slomp CP (2015) The nitrogen isotope composition of sediments from the proto-North Atlantic during Oceanic Anoxic Event 2. *Paleoceanography* 30(7):923-937.
12. Rau GH, Arthur MA, & Dean WE (1987) $^{15}N/^{14}N$ variations in Cretaceous Atlantic sedimentary sequences: implication for past changes in marine nitrogen biogeochemistry. *Earth Planet Sc. Lett.* 82(3–4):269-279.
13. Kuypers MMM, van Breugel Y, Schouten S, Erba E, & Sinninghe Damsté JS (2004) N_2-fixing cyanobacteria supplied nutrient N for Cretaceous oceanic anoxic events. *Geology* 32(10):853-856.
14. Junium CK & Arthur MA (2007) Nitrogen cycling during the Cretaceous, Cenomanian-Turonian Oceanic Anoxic Event II. *Geochem. Geophy. Geosy.* 8(3):Q03002.
15. Higgins MB, Robinson RS, Husson JM, Carter SJ, & Pearson A (2012) Dominant eukaryotic export production during ocean anoxic events reflects the importance of recycled NH_4^+. *P. Natl. Acad. Sci. USA* 109(7):2269-2274.
16. Junium CK, Dickson AJ, & Uveges BT (2018) Perturbation to the nitrogen cycle during rapid Early Eocene global warming. *Nat. Commun.* 9(1):3186.
17. Trabucho-Alexandre J, *et al.* (2010) The mid-Cretaceous North Atlantic nutrient trap: Black shales and OAEs. *Paleoceanography* 25(4):PA4201.
18. Ridgwell A, *et al.* (2007) Marine geochemical data assimilation in an efficient Earth System Model of global biogeochemical cycling. *Biogeosciences* 4(1):87-104.

19. Tsandev I & Slomp CP (2009) Modeling phosphorus cycling and carbon burial during Cretaceous Oceanic Anoxic Events. *Earth Planet. Sci. Lett.* 286(1):71-79.
20. Flögel S*, et al.* (2011) Simulating the biogeochemical effects of volcanic CO_2 degassing on the oxygen-state of the deep ocean during the Cenomanian/Turonian Anoxic Event (OAE 2). *Earth Planet Sc. Lett.* 305(3-4):371-384.
21. Konovalov SK, Ivanov LI, & Samodurov AS (2000) Oxygen, nitrogen and sulphide fluxes in the Black Sea. *Mediter. Mar. Sci.* 1(2):41-59.
22. Fennel K, Follows M, & Falkowski PG (2005) The co-evolution of the nitrogen, carbon and oxygen cycles in the Proterozoic ocean. *Am J. Sci.* 305(6-8):526-545.
23. Saltzman MR (2005) Phosphorus, nitrogen, and the redox evolution of the Paleozoic oceans. *Geology* 33(7):573-576.
24. Lenton TM & Watson AJ (2000) Redfield revisited: 1. Regulation of nitrate, phosphate, and oxygen in the ocean. *Global Biogeochem. Cy.* 14(1):225-248.
25. Monteiro FM, Pancost RD, Ridgwell A, & Donnadieu Y (2012) Nutrients as the dominant control on the spread of anoxia and euxinia across the Cenomanian-Turonian oceanic anoxic event (OAE2): Model-data comparison. *Paleoceanography* 27(4):PA4209.
26. Clarkson MO*, et al.* (2018) Uranium isotope evidence for two episodes of deoxygenation during Oceanic Anoxic Event 2. *P. Natl. Acad. Sci. USA* 115(12):2918-2923.
27. Blättler CL, Jenkyns HC, Reynard LM, & Henderson GM (2011) Significant increases in global weathering during Oceanic Anoxic Events 1a and 2 indicated by calcium isotopes. *Earth Planet. Sc. Lett.* 309(1-2):77-88.
28. House WA & Denison FH (2002) Total phosphorus content of river sediments in relationship to calcium, iron and organic matter concentrations. *Sci .Total Environ.* 282-283:341-351.
29. Van Cappellen P & Ingall ED (1994) Benthic phosphorus regeneration, net primary production, and ocean anoxia: A model of the coupled marine biogeochemical cycles of carbon and phosphorus. *Paleoceanography* 9(5):677-692.
30. Ruvalcaba Baroni I, Tsandev I, & Slomp CP (2014) Enhanced N_2-fixation and NH^{4+} recycling during oceanic anoxic event 2 in the proto-North Atlantic. *Geochem. Geophy. Geosy.* 15:GC005453.
31. Tuite ML, Jr. & Macko SA (2013) Basinward nitrogen limitation demonstrates role of terrestrial nitrogen and redox control of δ15N in a Late Devonian black shale. *Geology* 41(10):1079-1082.
32. Buick R (2007) Did the Proterozoic 'Canfield Ocean' cause a laughing gas greenhouse? *Geobiology* 5(2):97-100.
33. Freing A, Wallace DWR, & Bange HW (2012) Global oceanic production of nitrous oxide. *Phil. Trans. R. Soc. B* 367(1593):1245-1255.
34. Heimhofer U*, et al.* (2018) Vegetation response to exceptional global warmth during Oceanic Anoxic Event 2. *Nat. Commun.* 9(1):3832.
35. Schmidtko S, Stramma L, & Visbeck M (2017) Decline in global oceanic oxygen content during the past five decades. *Nature* 542:335.
36. Bopp L*, et al.* (2013) Multiple stressors of ocean ecosystems in the 21st century: projections with CMIP5 models. *Biogeosciences* 10(10):6225-6245.

37. Bristow LA, *et al.* (2016) N_2 production rates limited by nitrite availability in the Bay of Bengal oxygen minimum zone. *Nature Geosci.* 10:24.
38. Hansell DA, Bates NR, & Olson DB (2004) Excess nitrate and nitrogen fixation in the North Atlantic Ocean. *Mar. Chem.* 84(3–4):243-265.
39. Locarnini RA, *et al.* (2013) NOAA Atlas NESDIS 73 WORLD OCEAN ATLAS 2013, Volume 1: Temperature.
40. Henson SA, *et al.* (2011) A reduced estimate of the strength of the ocean's biological carbon pump. *Geophys. Res. Lett.* 38(4).
41. DeVries T, Deutsch C, Rafter PA, & Primeau F (2013) Marine denitrification rates determined from a global 3-D inverse model. *Biogeosciences* 10(4):2481-2496.

Figure Legends

Figure 1: Response of marine biogeochemistry

Response of ocean biogeochemistry to an increase in oceanic phosphate inventory for the Cenomanian simulations (pCO_2 at 1,120 ppmv). A) Ocean redox state with total oxygen content (O_2) of the ocean, extent of photic zone euxinia (PZE), extent of pure sea floor anoxia (< 1 nM O_2), and rate of export production; B) Concentration of nitrate, ammonium, total fixed nitrogen (NO_3^- + NH_4^+), and phosphate concentration (in µmol N l^{-1}; multiplied by the Redfield N:P ratio); C) DIN_{xs} (DIN_{xs} = NO_3^- + NH_4^+ - 16 x PO_4^{3-}) (38), and D) Contribution of nitrogen fixation, ammonium assimilation, and nitrate assimilation to export production. Dashed lines represent values in modern-day simulation (1 x CO_2, 1 x PO_4^{3-} , and modern geography, ocean circulation and temperature). The 2 x PO_4^{3-} simulation has the best fit with proxy data for OAE 2 (25).

Figure 2: Marine N-cycle during OAE 2 (4 x CO_2; 2 x PO_4^{3-})

A) Spatial distribution of the relative contribution to export production of N fixation (top), NH_4^+ assimilation (middle), and NO_3^- assimilation (bottom). Green ⊕ symbols reflect proxy records with a positive average $\delta^{15}N_{bulk}$ value across OAE 2, while pink ⊖ symbols reflect a negative average $\delta^{15}N_{bulk}$ value. Numbers refer to sites listed in table S1 (see SI appendix for details); and B) Zonally averaged vertical concentration profiles of O_2 (top), NH_4^+ (middle), and NO_3^- (bottom). Both panels present model results using the OAE 2 analog simulation (Cenomanian paleography, 4 x CO_2; 2 x PO_4^{3-}).

Figure 3: Schematic of the marine nitrogen cycle's response to oceanic de-oxygenation

The transition from an oxic, nitrate-dominated ocean to an anoxic, ammonium-dominated ocean. Also shown is DIN_{xs} ($DIN_{xs} = NO_3^- + NH_4^+ - 16 \times PO_4^{3-}$) (38). During OAE 2, the intermediate N-deficit state may have prevailed.

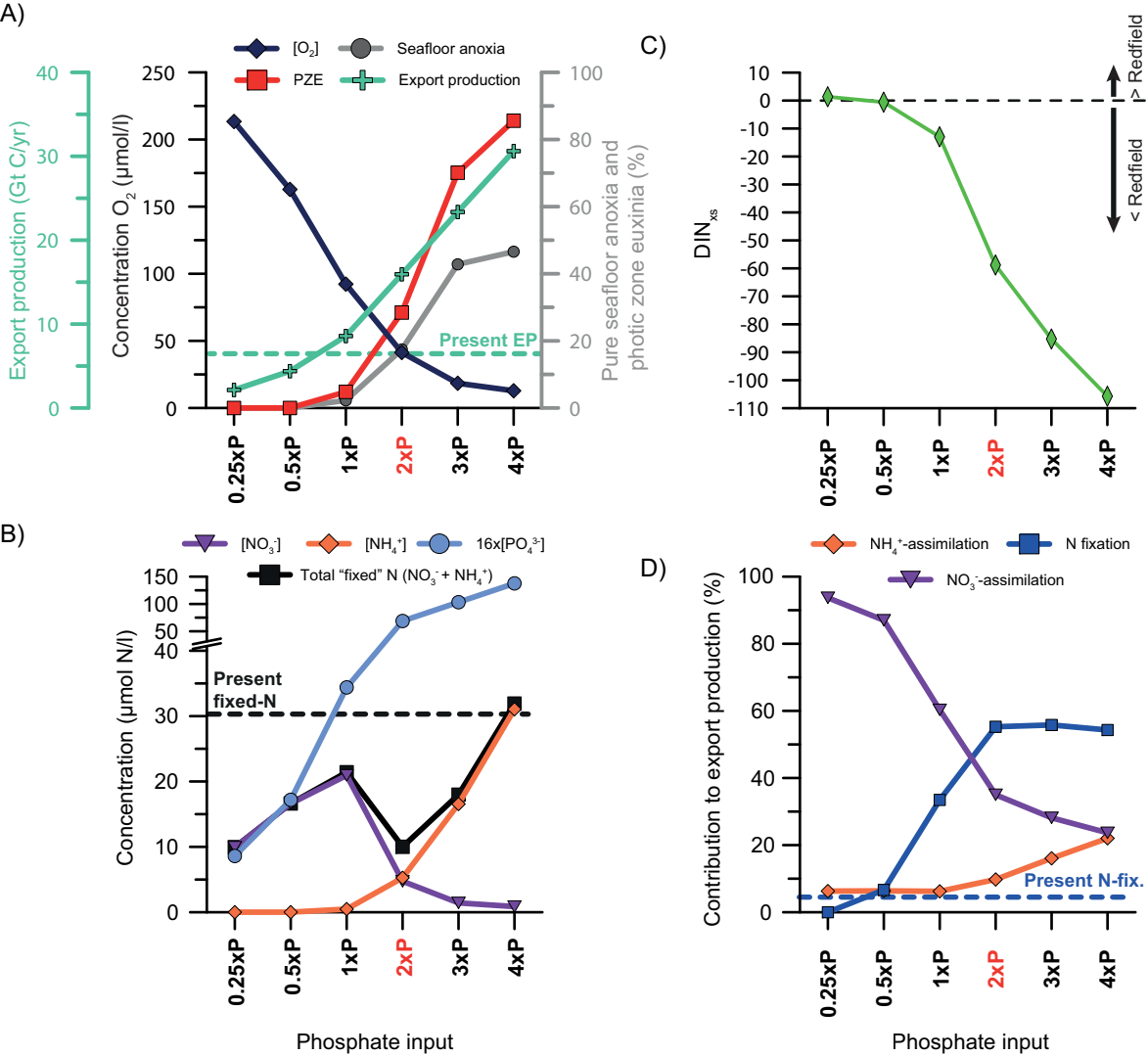
A)
[O2]
Seafloor anoxia
PZE
Export production
Export production (Gt C/yr)
Concentration O2 (µmol/l)
Pure seafloor anoxia and photic zone euxinia (%)
Present EP
0.25xP
0.5xP
1xP
2xP
3xP
4xP
B)
[NO3-]
[NH4+]
16x[PO43-]
Total "fixed" N (NO3- + NH4+)
Concentration (µmol N/l)
Present fixed-N
Phosphate input
C)
DINxs
> Redfield
< Redfield
D)
NH4+-assimilation
N fixation
NO3--assimilation
Contribution to export production (%)
Present N-fix.
Phosphate input

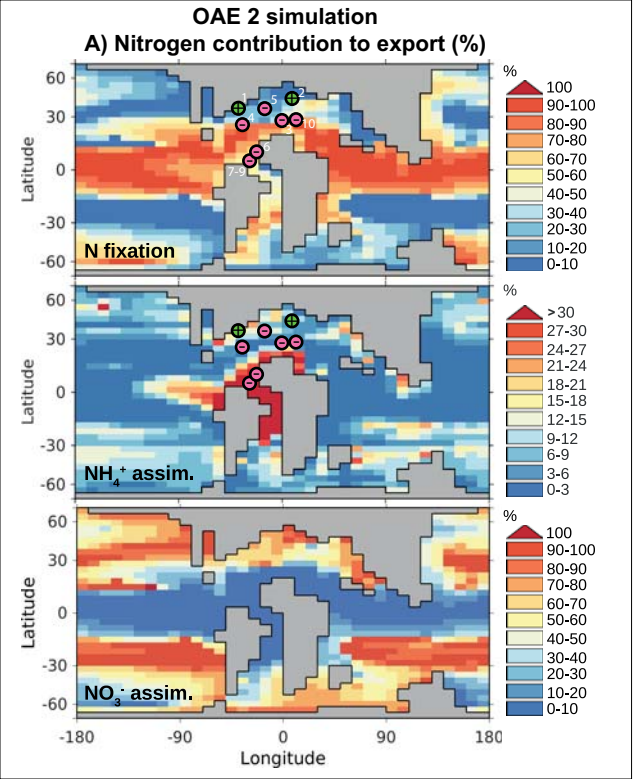
OAE 2 simulation
A) Nitrogen contribution to export (%)
N fixation
NH4+ assim.
NO3- assim.
Latitude
Longitude
%
100
90-100
80-90
70-80
60-70
50-60
40-50
30-40
20-30
10-20
0-10
>30
27-30
24-27
21-24
18-21
15-18
12-15
9-12
6-9
3-6
0-3

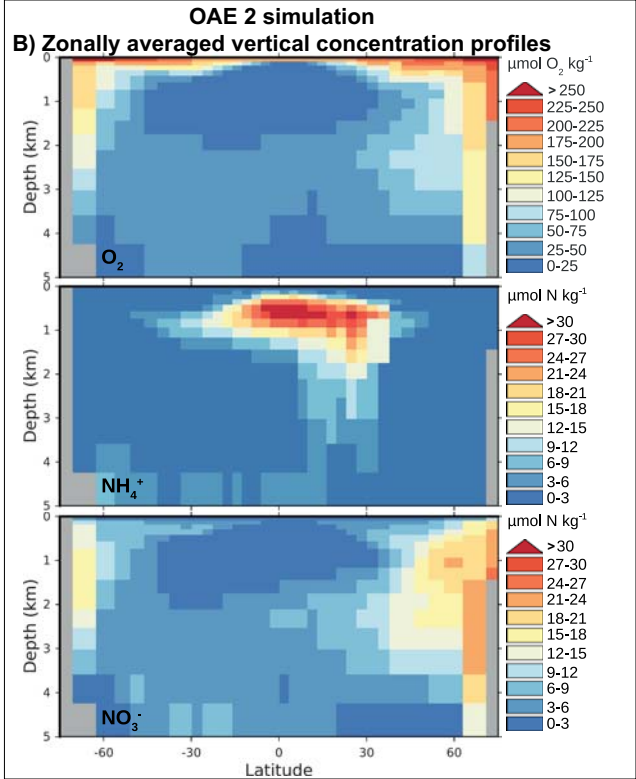
OAE 2 simulation
B) Zonally averaged vertical concentration profiles
O2
NH4+
NO3-
Depth (km)
Latitude
µmol O2 kg-1
µmol N kg-1
>250
225-250
200-225
175-200
150-175
125-150
100-125
75-100
50-75
25-50
0-25
>30
27-30
24-27
21-24
18-21
15-18
12-15
9-12
6-9
3-6
0-3

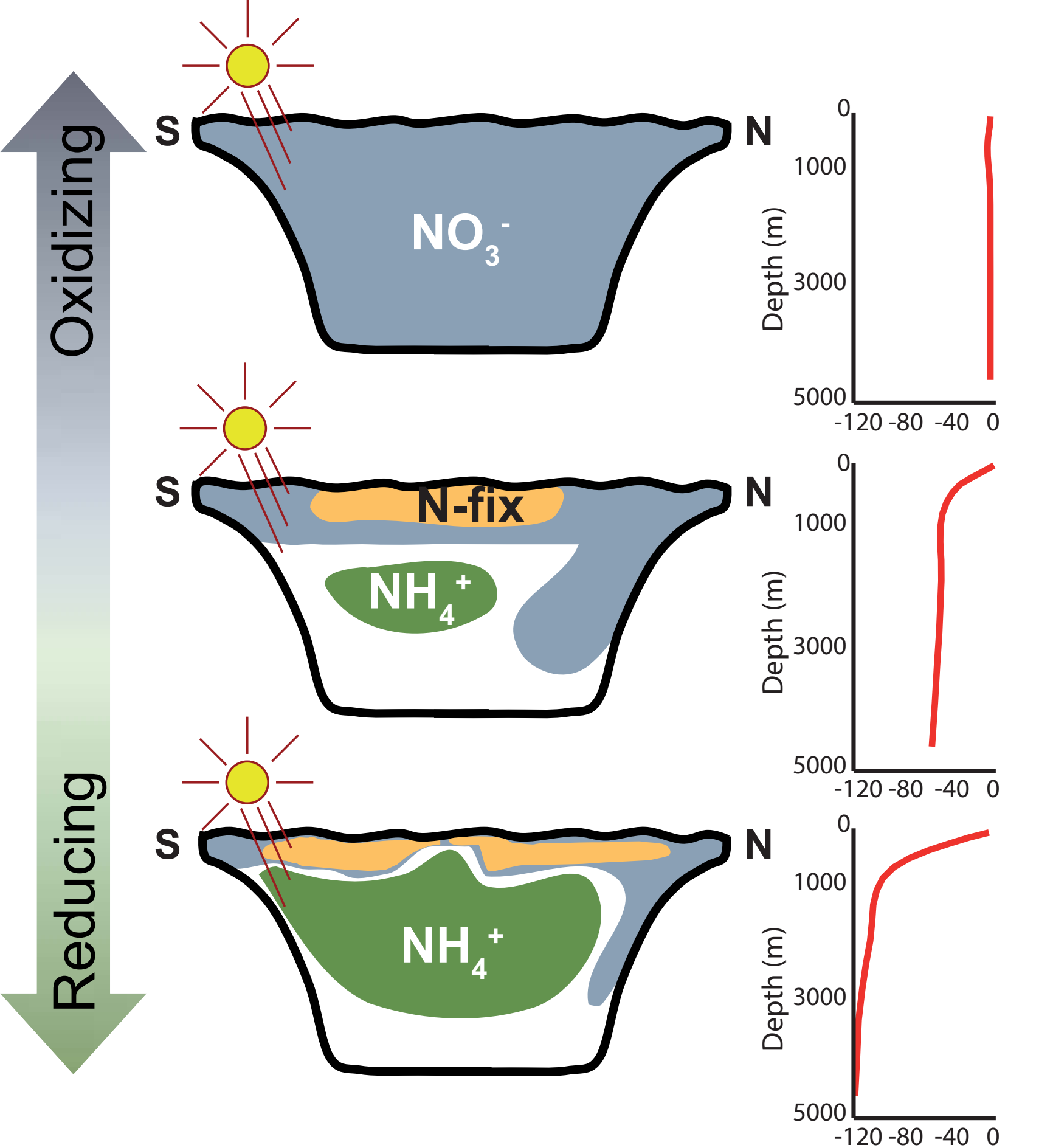
Oxidizing
Reducing
S
N
NO_3^-
N-fix
NH_4^+
NH_4^+
0
1000
3000
5000
Depth (m)
-120 -80 -40 0
DIN_{xs} (μmol N/l)

Table 1; Marine biogeochemistry for the modern and (pre-)OAE 2

Variable	Unit	Modern (Observed)	Modern (GENIE)	Pre-OAE 2 (GENIE)	OAE 2 (GENIE)
Atmospheric CO_2		1 x CO_2	1 x CO_2	2 x CO_2	4 x CO_2
Oceanic phosphate		1 x PO_4^{3-}	1 x PO_4^{3-}	1 x PO_4^{3-}	2 x PO_4^{3-}
Anoxia					
Global ocean anoxia	% volume	< 0.1 (ref. 39)	< 0.1	2	11
Seafloor anoxia	% area	<0.1 (ref. 39)	< 0.1	2	17
Euxinia					
Global ocean euxinia	% volume	<0.1 (ref. 39)	< 0.1	4	28
Photic zone euxinia	% area	<0.1 (ref. 39)	< 0.1	0.5	11
Biological rates					
Export Production	Gt C yr^{-1}	5-20 (ref. 40)	7	8	16
Nitrification	Tg N yr^{-1}		2312	3152	6050
Denitrification	Tg N yr^{-1}	120-240 (ref. 41)	114	812	3249
Global contribution to export					
NO_3-assimilation	%		87	65	35
N_2-fixation	%		5	28	55
NH_4^+-assimilation	%		8	6	10
Global contribution to remineralization					
O_2-respiration	%		99	90	72
Denitrification	%		1	8	16
SO_4^{2-}-reduction	%		< 0.1	2	12

PNAS
www.pnas.org

Supplementary Information for "Fundamentally different global marine nitrogen cycling in response to extreme ocean deoxygenation"

B. David A. Naafs[1,+], Fanny M. Monteiro[2], Ann Pearson[3], Meytal B. Higgins[4], Rich D. Pancost[1], and Andy Ridgwell[2,5]

[1]Organic Geochemistry Unit, School of Chemistry, School of Earth Sciences, the Cabot Institute for the Environment, University of Bristol, Bristol, UK
[2]School of Geographical Sciences, University of Bristol, Bristol, UK
[3]Department of Earth and Planetary Sciences, Harvard University, Cambridge, USA
[4]ExxonMobil Research & Engineering, Annandale, USA
[5]Department of Earth and Planetary Sciences, University of California-Riverside, Riverside, CA, USA

[+]David Naafs
Email: david.naafs@bristol.ac.uk

This PDF file includes:

Supplementary Information Text

1. Nitrogen cycle in GENIE

We used the already published OAE 2 data-constrained Cenomanian paleogeography configuration of the GENIE model (1), with simulations conducted at 4x pre-industrial atmospheric CO_2 concentrations, and a range of different oceanic phosphate inventories (0.25 to 4 times modern PO_4^{3-}). Although we could have explored the effects of other biogeochemical variables such as imposing changes on atmospheric pO_2 and hence ocean dissolved oxygen concentrations directly, OAEs are widely regarded as being characterized by high levels of pCO_2 (2) and are inferred to be characterized by a higher-than-modern oceanic phosphate. This increased P inventory resulted from extensive submarine volcanism (2, 3) and hence increased terrestrial rock (and apatite mineral) weathering rates (4), in combination with a decreased ocean sink as a consequence of benthic P regeneration under sedimentary anoxia (5). All model scenarios were run for 20 kyr to steady state.

For the model configuration used for OAE 2, see Monteiro et al. (1). Genie biogeochemistry accounted for carbon, phosphorous, nitrogen, oxygen, and sulfur cycling as described by Monteiro et al. (1), including equations and parameters values for ocean productivity, a dynamical threshold for oligotrophy for nitrogen fixation, and remineralisation of organic matter (DOM and POM pools) via oxygen, nitrate and sulphate reductions. In the absence of a consensus on ocean sulphate concentrations during the Cretaceous and OAEs, we used modern sulphate concentrations as the initial concentration in all simulations (29,160 mM). The model's nitrogen cycle includes ammonium and nitrate assimilations (with a preference towards ammonium assimilation). Nitrogen fixation is constrained to the surface layer of the ocean, whereas remineralisation of organic nitrogen into ammonium, and nitrification of ammonium into nitrate, are present in the whole water column (with rates depending on the ocean redox state).

Here, we updated the marine N cycle to allow the global nitrogen fixation rate in the modern ocean to fit more recent observations and introduced a limitation of nitrification by oxygen in addition to ammonium (see section 2.1 and 2.2 for details). All simulations were run using this updated code of the marine N cycle.

To estimate the different contributions of N sources onto export production, we assumed that global scale export production is equivalent to new production, which is the sum of N_2 fixation with NO_3^- and NH_4^+ new production (represented by DIN new production in figure S1). Export production includes here the sum of the sinking of particulate organic matter (POM) and the mixing of dissolved organic matter (DOM) out of the photic zone. In the modern ocean, new production/export

67 production is dominated by the uptake of NO_3^-, because $NH_4^+{}_{new}$ is negligible as most
68 of NH_4^+ is oxidized in the deep ocean and N_2 fixation is relatively small. In an anoxic
69 ocean, contribution to new production/export production by N_2 and potentially NH_4^+
70 become important because low oxygen content promotes denitrification (hence
71 increasing N_2 fixation) and accumulation of NH_4^+ in the deep ocean. Also included in
72 the model is denitrification, which converts organic nitrogen and NO_3^- into NH_4^+ and
73 N_2 (g) when oxygen content is low (below 40 μmol O_2 l^{-1}).
74

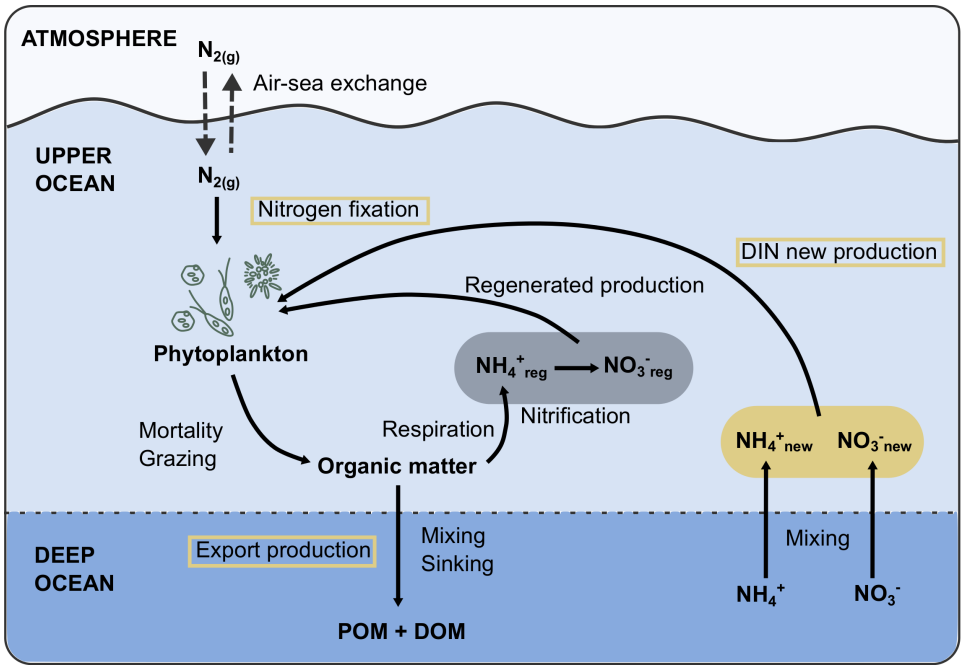

***Figure S1**: Schematics of the nitrogen cycle in GENIE, distinguishing new production from regenerated production.*

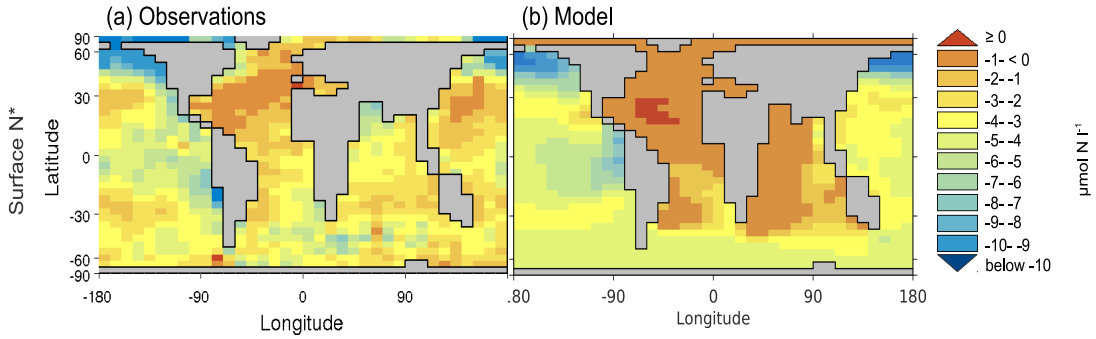

***Figure S2**: Comparison of modern surface N* between a) Observations from the World Ocean Atlas 2001 (6) and b) results of the pre-industrial simulation of GENIE with a modern geography (1 x CO_2; 1 x PO_4^{3-}).*

1.1 Nitrogen fixation rate

To increase the global rate of nitrogen fixation and match more recent modern ocean estimates that range between 50 and 350 TgN/yr (7-11), for the modern day simulations we reduced the half-saturation constant for iron limitation of diazotrophs to 0.5 nmol Fe l^{-1} and increased the threshold of oxygen below which denitrification occurs in the water column to 40 µmol O_2 l^{-1} (previously 1.0 nmol Fe l^{-1} and 30 µmol O_2 l^{-1}, respectively). These had the effect of increasing global nitrogen fixation rates to 115 TgN yr^{-1} for the preindustrial run (65 TgN yr^{-1} in the model setup of Monteiro et al., (1)). A comparison between modeled and observed oceanic distribution of N*, demonstrated a good agreement (Fig. S2). N*= DIN – 16 x PO_4^{3-}, where DIN is the total concentration of inorganic nitrogen DIN = NH_4^+ + NO_3^-.

For the Mesozoic simulations we assume no trace metal (e.g., Fe) limitation on phytoplankton (including diazotrophs). In the modern ocean, iron limitation on diazotrophs has been suggested to potentially limit global rate of N_2-fixation (12). However recent evidence suggest that iron limitation influences regional patterns of N_2 fixation and that rates of N loss govern basin-scale patterns (hence global N_2 fixation rate) (13). For our Mesozoic simulations we assume no iron limitation on phytoplankton because iron was likely more abundant during OAEs as a result of an increased input due to submarine volcanism (3, 14, 15) and weathering (4, 16, 17) and because anoxia increases iron bioavailability (18). In addition, in a reducing ocean, diazotrophs might use alternative nitrogenases, allowing for higher rates of N_2-fixation despite changes in the bioavailability of trace elements such as Mo (19).

1.2 Nitrification

GENIE uses nitrification as the overall oxidizing process of ammonium (NH_4^+) into nitrate (NO_3^-), as it does not explicitly represent nitrite (NO_2^-). The model version used previously in Monteiro et al. (1) accounts for the limitation of nitrification by ammonium (20). Here we added the effect of oxygen limitation on nitrification, which could be important for an OAE-like ocean where oxygen concentrations can be regionally very low. For this modification, we used the Michaelis-Menten approach to a two-substrate reaction to estimate the rate of nitrification (Λ^{Nitri}) (21):

$$\Lambda^{Nitri} = V_{max}^{Nitri} \frac{O_2 \times NH_4^+}{\left(k_{O2}^{Nitri} \times k_{NH4+}^{Nitri}\right) + \left(k_{O2}^{Nitri} \times NH_4^+\right) + \left(k_{NH4+}^{Nitri} \times O_2\right) + \left(O_2 \times NH_4^+\right)} min\left(NH_4^+; \frac{16}{138} O_2\right)$$

where V_{max}^{Nitri} is the maximum constant rate of nitrification; k_{O2}^{Nitri} and k_{NH4+}^{Nitri} are the half saturation constant for oxygen and ammonium, respectively. We also assumed

that the dissociation constant (k_{NH4+O2}^{Nitri}) is equivalent to the product of k_{O2}^{Nitri} and k_{NH4+}^{Nitri} based on equation 6 of Alberty (21), and assuming that the affinity of the enzyme for NH_4^+ is not dependent on the concentration of O_2, a reasonable assumption for this system (22). The new nitrification parameters were tuned to give a realistic global nitrification rate with a NH_4^+ vertical profile of around 0.01 μmol N kg^{-1} below the photic zone (23) (see Table S1 for parameter values).

Table S1: GENIE parameter values of nitrification

Symbol	Description	Unit	Value	Observed
V_{max}^{Nitri}	Maximum constant rate of nitrification	d^{-1}	0.02	0.02-2 (ref. (24-26))
k_{NH4+}^{Nitri}	Half-saturation constant for ammonium	μmol N l^{-1}	0.01	0.01-100 (ref. (24, 27))
k_{O2}^{Nitri}	Half-saturation constant for oxygen	μmol N l^{-1}	0.02	0.02-20 (ref. (24))

1.3. Contribution of different nitrogen sources to export production

Export production in the modern ocean is mostly fueled by nitrate because of the dominance of NO_3^- in upwelling waters and relatively low rates of N_2-fixation. However, in low-oxygen environments such as during OAEs, N_2 and NH_4^+ can become important sources of nitrogen for export production because of the higher rate of denitrification (increasing N_2-fixation and reducing NO_3^-) and relatively lower rate of nitrification (oxidizing NH_4^+ into NO_3^-) below the photic zone within the widespread OMZs. To estimate the relative contribution of NO_3^-, NH_4^+ and N_2 to export production, we first assumed export production to be equivalent to new production on the global scale. New production is the part of primary production fueled by non-regenerated nutrients (either by DIN coming from below the photic-zone or via N_2-fixation). We represented new production by DIN in the model as the uptake by phytoplankton of "new" DIN where new DIN is set to the concentration of DIN below a certain depth following Yool et al. (25) (referred as "Newification"). Here we generalized Yool et al. (25)'s concept to account for both NH_4^+ and NO_3^--driven new production, the former being negligible in the modern ocean (except for potentially above oxygen minimum zones), but not for OAEs.

The diagnostic equations for new NH_4^+ ($NH_4^+{}_{new}$) and new NO_3^- ($NO_3^-{}_{new}$) are

as follows:

$$\frac{dNH_{4\,new}^{+}}{dt} = -\underbrace{Uptake(NH_{4\,new}^{+})}_{NH_4^+\ new\ production} + \underbrace{\Omega(z) \times\ NH_4^+}_{\text{“Newification”}}$$

$$\frac{dNO_{3\,new}^{-}}{dt} = -\underbrace{Uptake(NO_{3\,new}^{-})}_{NO_3^-\ new\ production} + \Omega(z) \times\ NO_3^-$$

where Uptake ($NH_4^+{}_{new}$) and Uptake ($NO_3^-{}_{new}$) are the uptake by phytoplankton of $NH_4^+{}_{new}$ and $NO_3^-{}_{new}$, respectively, which represent NH_4^+ and NO_3^- new productions and direct estimates of contributions to export production. Ω(z) x NH_4^+ and Ω(z) x NO_3^- are the newification terms as defined by Yool et al. (25), where $NH_4^+{}_{new}$ and $NO_3^-{}_{new}$ are set to NH_4^+ and NO_3^- concentrations below a specific depth (z). Here we took (z) to be the bottom of the photic zone. Finally, we defined the uptake by phytoplankton of $NH_4^+{}_{new}$ and $NO_3^-{}_{new}$ as:

$$Uptake(NH_{4\,new}^{+}) = \frac{NH_{4\,new}^{+}}{NH_4^+ + NO_3^-} Uptake(NH_4^+)$$

$$Uptake(NO_{3\,new}^{-}) = \frac{NO_{3\,new}^{-}}{NH_4^+ + NO_3^-} Uptake(NO_3^-).$$

Uptake (NH_4^+) and Uptake (NO_3^-) are the uptake rates of NH_4^+ and NO_3^- by phytoplankton, where we assumed that NH_4^+ is preferentially utilized:

$$Uptake(NH_4^+) = \min\left(\Gamma^{Phy}; NH_4^+\right)$$

$$Uptake(NO_3^-) = \Gamma^{Phy} - Uptake(NH_4^+).$$

Γ^{phy} is the net depletion of nutrient by non-diazotroph phytoplankton in nitrogen unit as defined in Monteiro et al. (1):

$$\Gamma^{Phy} = V_{max}^{Phy} \gamma^T \gamma^I \min\left(\frac{PO_4^{3-}}{PO_4^{3-} + K_p}; \frac{DIN}{DIN + K_N}\right) \min\left(16\ \times\ PO_4^{3-}; DIN\right).$$

Export production here accounts for the combination of the export of particulate organic matter (POM) and the mixing out of the photic zone of dissolved organic matter (DOM). GENIE only prescribes the amount of POM export. We thus calculated the amount of DOM mixing out of the photic zone assuming that the total new production (N_2 fixation + NH_4^+ new production + NO_3^- new production) is equal to the total export production (POM export + DOM mixing).

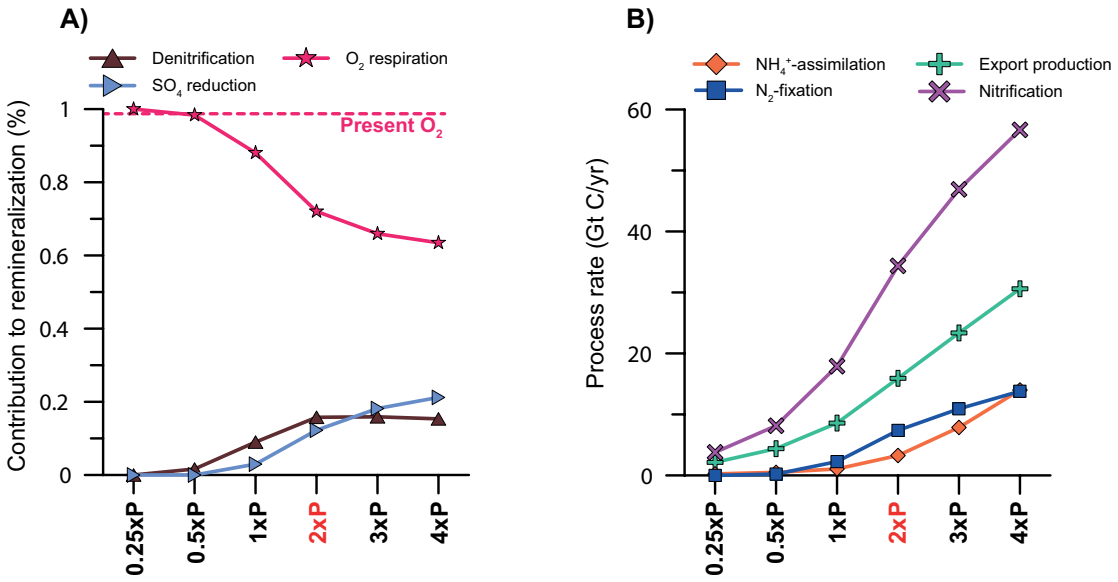

***Figure S3**; response of ocean biogeochemistry (contribution to remineralization; left) and marine N-cycle (process rates; right) to changes in oceanic phosphate content in the Cenomanian simulations run with 4 x CO_2.*

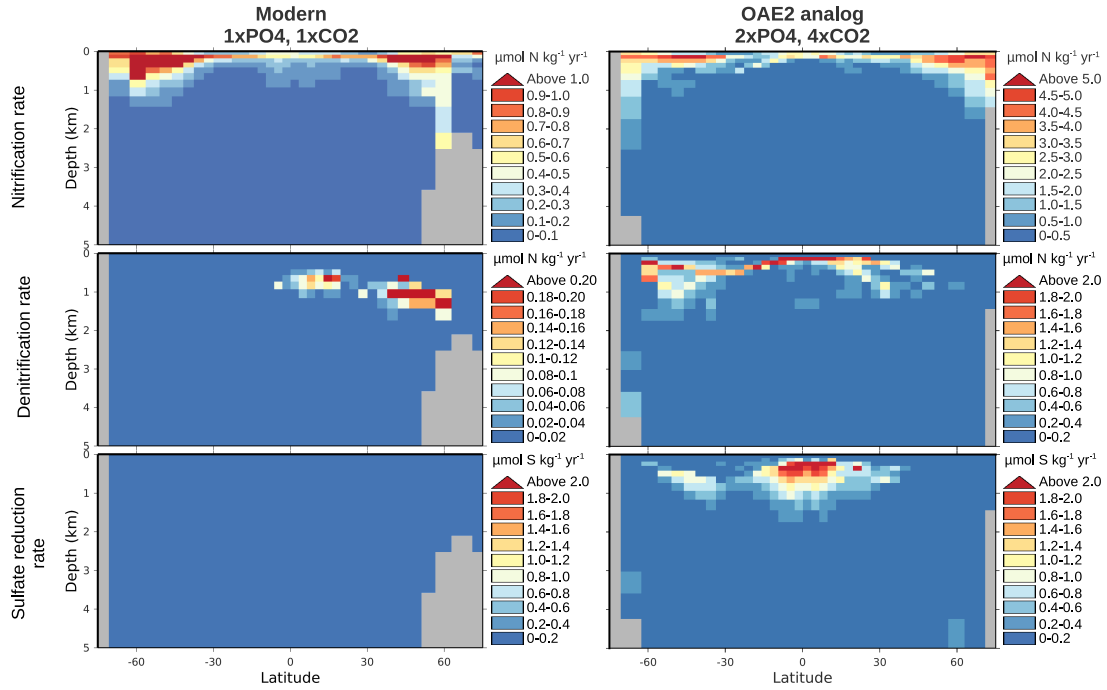

***Figure S4**; Globally integrated vertical profiles of the nitrification, denitrification, and sulfate reduction rates in the global ocean in the modern (left) and OAE 2 analog simulations (right).*

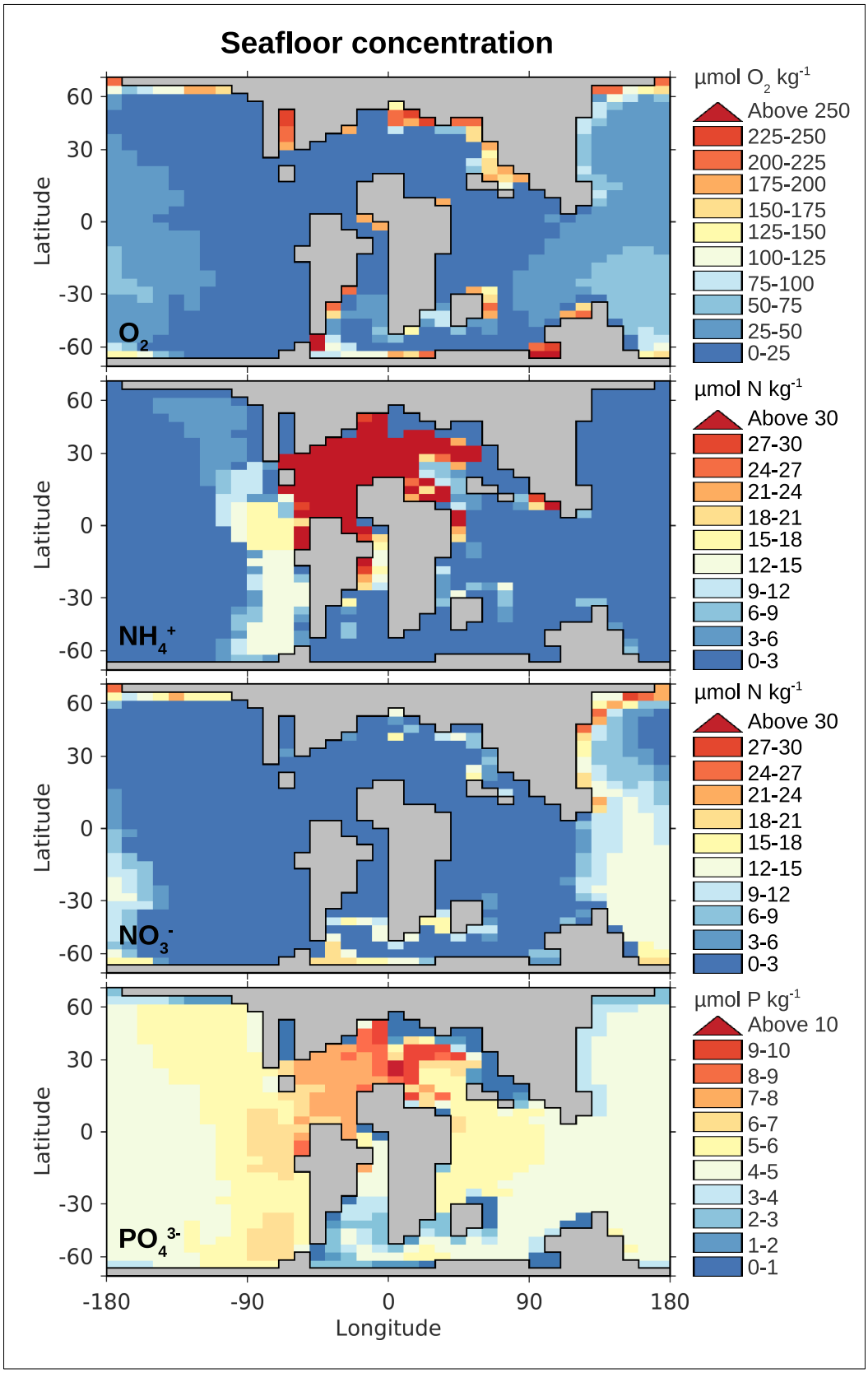

***Figure S5**; Concentrations of oxygen, ammonium, nitrate, and phosphate in bottom waters for the OAE 2 analog simulation.*

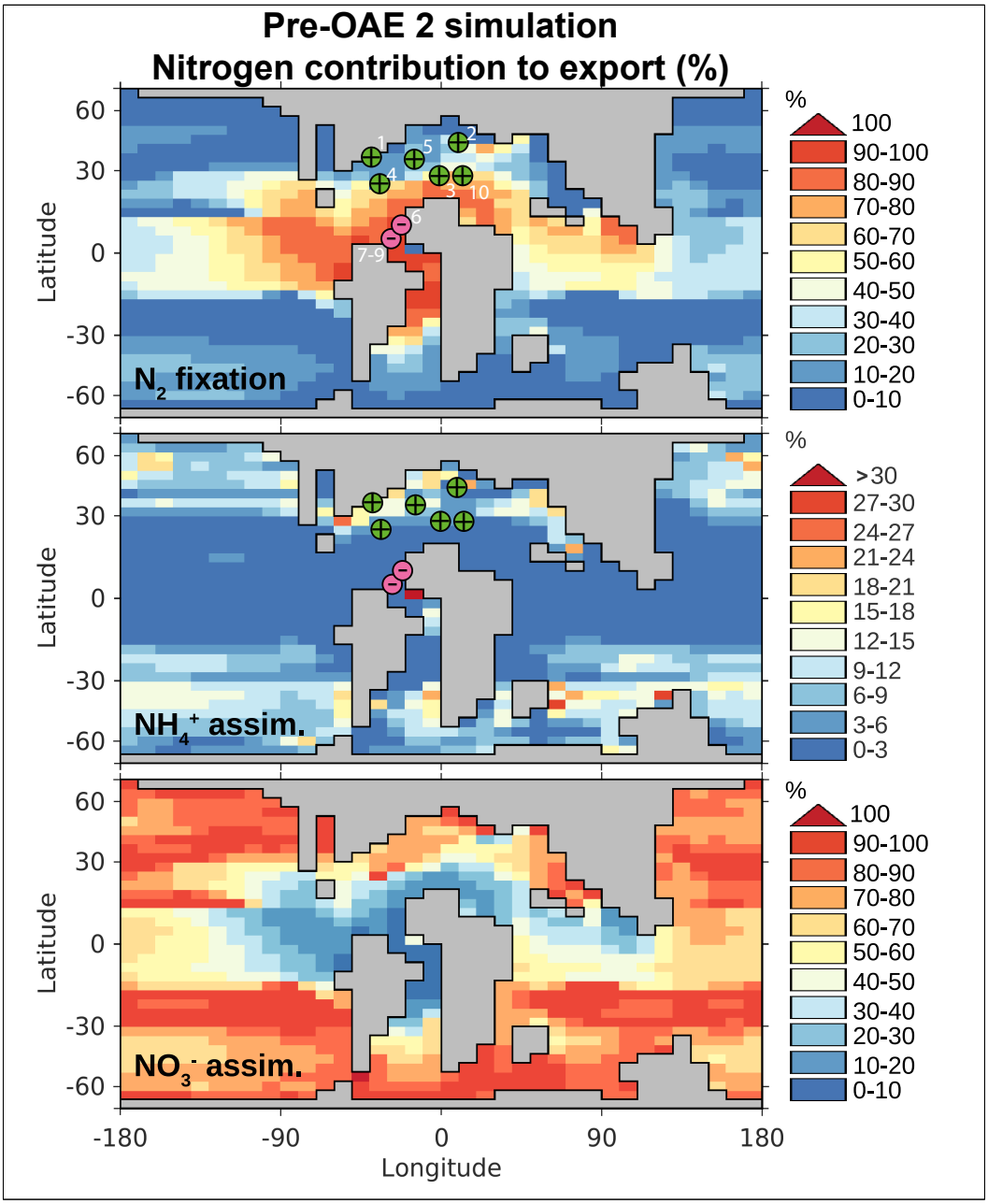

194

195 ***Figure S6**: Spatial distribution of the relative contribution to export production of N_2*

196 *fixation, NH_4^+ assimilation, and NO_3^- assimilation for the pre-OAE 2 simulation. Green*

197 *⊕ symbols reflect proxy records with a positive average $\delta^{15}N_{bulk}$ value across OAE 2,*

198 *while pink ⊖ symbols reflect a negative average $\delta^{15}N_{bulk}$ value. Numbers refer to*

199 *sites listed in table S1*

200

Table S2; Nitrogen stable isotope records that contain OAE 2											
	pre-OAE 2 (Fig. S6)					OAE 2 (Fig. 2)					
Site	**Average**	**Symbol**	**St.dev.**	**Min**	**Max**	**Average**	**Symbol**	**St.dev.**	**Min**	**Max**	**Reference**
1. Bass River	1.3	⊕	0.4	0.3	1.7	1.3	⊕	0.4	-0.2	2.0	(28)
2. Wunstorf	0.9	⊕	0.4	0.6	1.5	0.9	⊕	1.3	-1.5	3.3	(28)
3. Site 641	2.3	⊕	0.4	1.8	2.9	-1.0	⊖	2.7	-2.7	3.0	(28)
4. Site 386	2.1	⊕	0.3	1.8	2.6	-2.1	⊖	1.3	-2.8	1.1	(28)
5. Site 1276	1.7	⊕	0.6	1.1	2.8	-1.0	⊖	1.5	-2.8	2.7	(28)
6. Site 367	-1.3	⊖	0.4	-1.7	-0.8	-1.7	⊖	0.7	-2.3	0.2	(29)
7. Site 1258	-1.1	⊖	0.7	-1.9	-0.1	-1.5	⊖	0.6	-2.5	-0.4	(30)
8. Site 1260	-0.6	⊖	0.3	-0.9	-0.4	-1.9	⊖	0.8	-2.6	-0.8	(31)
9. Site 1261	-1.1	⊖	0.5	-2.0	-0.5	-2.3	⊖	0.6	-3.4	-0.9	(31)
10. Gorgo Cerbara	>0	⊕	-	-	-	-1.9	⊖	0.5	-2.7	-0.7	(32)

201

Supplementary references

1. Monteiro FM, Pancost RD, Ridgwell A, & Donnadieu Y (2012) Nutrients as the dominant control on the spread of anoxia and euxinia across the Cenomanian-Turonian oceanic anoxic event (OAE2): Model-data comparison. *Paleoceanography* 27(4):PA4209.
2. Naafs BDA*, et al.* (2016) Gradual and sustained carbon dioxide release during Aptian Oceanic Anoxic Event 1a. *Nature Geosci.* 9(2):135-139.
3. Turgeon SC & Creaser RA (2008) Cretaceous oceanic anoxic event 2 triggered by a massive magmatic episode. *Nature* 454(7202):323-326.
4. Lechler M, Pogge von Strandmann PAE, Jenkyns HC, Prosser G, & Parente M (2015) Lithium-isotope evidence for enhanced silicate weathering during OAE 1a (Early Aptian Selli event). *Earth Planet. Sc. Lett.* 432:210-222.
5. Van Cappellen P & Ingall ED (1994) Benthic phosphorus regeneration, net primary production, and ocean anoxia: A model of the coupled marine biogeochemical cycles of carbon and phosphorus. *Paleoceanography* 9(5):677-692.
6. Conkright ME*, et al.* (2002) *World Ocean Atlas 2001: Objective analyses, data statistics, and figures: CD-ROM documentation* (US Department of Commerce, National Oceanic and Atmospheric Administration, National Oceanographic Data Center, Ocean Climate Laboratory).
7. Luo YW*, et al.* (2012) Database of diazotrophs in global ocean: abundance, biomass and nitrogen fixation rates. *Earth Syst. Sci. Data* 4(1):47-73.
8. Monteiro FM, Follows MJ, & Dutkiewicz S (2010) Distribution of diverse nitrogen fixers in the global ocean. *Glob. Biogeochem. Cycles* 24(3):GB3017.
9. Somes CJ, Oschlies A, & Schmittner A (2013) Isotopic constraints on the pre-industrial oceanic nitrogen budget. *Biogeosciences* 10(9):5889-5910.
10. Großkopf T*, et al.* (2012) Doubling of marine dinitrogen-fixation rates based on direct measurements. *Nature* 488(7411):361-364.
11. Knapp AN, Casciotti KL, Berelson WM, Prokopenko MG, & Capone DG (2016) Low rates of nitrogen fixation in eastern tropical South Pacific surface waters. *Proc. Natl. Acad. Sci. U.S.A.* 113(16):4398-4403.
12. Falkowski PG (1997) Evolution of the nitrogen cycle and its influence on the biological sequestration of CO_2 in the ocean. *Nature* 387(6630):272-275.
13. Weber T & Deutsch C (2014) Local versus basin-scale limitation of marine nitrogen fixation. *Proc. Natl. Acad. Sci. U.S.A.* 111(24):8741-8746.
14. Tarduno JA*, et al.* (1991) Rapid Formation of Ontong Java Plateau by Aptian Mantle Plume Volcanism. *Science* 254(5030):399-403.
15. Bottini C, Cohen AS, Erba E, Jenkyns HC, & Coe AL (2012) Osmium-isotope evidence for volcanism, weathering, and ocean mixing during the early Aptian OAE 1a. *Geology* 40(7):583-586.
16. Blättler CL, Jenkyns HC, Reynard LM, & Henderson GM (2011) Significant increases in global weathering during Oceanic Anoxic Events 1a and 2 indicated by calcium isotopes. *Earth Planet. Sc. Lett.* 309(1-2):77-88.
17. Pogge von Strandmann PAE, Jenkyns HC, & Woodfine RG (2013) Lithium isotope evidence for enhanced weathering during Oceanic Anoxic Event 2. *Nature Geosci.* 6(8):668-672.
18. Saito MA, Sigman DM, & Morel FMM (2003) The bioinorganic chemistry of the ancient ocean: the co-evolution of cyanobacterial metal requirements and

biogeochemical cycles at the Archean–Proterozoic boundary? *Inorg. Chim. Acta* 356:308-318.
19. Zhang X, Sigman DM, Morel FMM, & Kraepiel AML (2014) Nitrogen isotope fractionation by alternative nitrogenases and past ocean anoxia. *P. Natl. Acad. Sci. USA*.
20. Fennel K, Follows M, & Falkowski PG (2005) The co-evolution of the nitrogen, carbon and oxygen cycles in the Proterozoic ocean. *Am J. Sci.* 305(6-8):526-545.
21. Alberty RA (1953) The Relationship between Michaelis Constants, Maximum Velocities and the Equilibrium Constant for an Enzyme-catalyzed Reaction. *J. Am. Chem. Soc.* 75(8):1928-1932.
22. Yool A (2011) Chapter one - Modeling the Role of Nitrification in Open Ocean Productivity and the Nitrogen Cycle. *Methods in Enzymology*, ed Klotz MG (Academic Press), Vol 486, pp 3-32.
23. Gruber N (2008) *The marine nitrogen cycle: overview and challenges* (San Diego, CA, USA: Elsevier) pp 1-50.
24. Bouskill N, Tang J, Riley W, & Brodie E (2012) Trait-Based Representation of Biological Nitrification: Model Development, Testing, and Predicted Community Composition. *Front. Microbiol.* 3:364.
25. Yool A, Martin AP, Fernandez C, & Clark DR (2007) The significance of nitrification for oceanic new production. *Nature* 447(7147):999-1002.
26. You J, Das A, Dolan EM, & Hu Z (2009) Ammonia-oxidizing archaea involved in nitrogen removal. *Water Res.* 43(7):1801-1809.
27. Martens-Habbena W, Berube PM, Urakawa H, de la Torre JR, & Stahl DA (2009) Ammonia oxidation kinetics determine niche separation of nitrifying Archaea and Bacteria. *Nature* 461(7266):976-979.
28. Ruvalcaba Baroni I, van Helmond NAGM, Tsandev I, Middelburg JJ, & Slomp CP (2015) The nitrogen isotope composition of sediments from the proto-North Atlantic during Oceanic Anoxic Event 2. *Paleoceanography* 30(7):923-937.
29. Kuypers MMM, van Breugel Y, Schouten S, Erba E, & Sinninghe Damsté JS (2004) N_2-fixing cyanobacteria supplied nutrient N for Cretaceous oceanic anoxic events. *Geology* 32(10):853-856.
30. Higgins MB, Robinson RS, Husson JM, Carter SJ, & Pearson A (2012) Dominant eukaryotic export production during ocean anoxic events reflects the importance of recycled NH_4^+. *P. Natl. Acad. Sci. USA* 109(7):2269-2274.
31. Junium CK & Arthur MA (2007) Nitrogen cycling during the Cretaceous, Cenomanian-Turonian Oceanic Anoxic Event II. *Geochem. Geophy. Geosy.* 8(3):Q03002.
32. Ohkouchi N, Kashiyama Y, Kuroda J, Ogawa NO, & Kitazato H (2006) The importance of diazotrophic cyanobacteria as primary producers during Cretaceous Oceanic Anoxic Event 2. *Biogeosciences* 3(4):467-478.